JOURNAL OF GEOPHYSICAL RESEARCH, VOL. 104, NO. D17, PAGES 21,569–21,577, SEPTEMBER 20, 1999

Impact of tropospheric aerosol absorption on ozone retrieval from backscattered ultraviolet measurements

O. Torres[1] and P. K. Bhartia

Laboratory for Atmospheres, NASA Goddard Space Flight Center, Greenbelt, Maryland

Abstract. The impact of tropospheric aerosols on the retrieval of column ozone amounts using space-borne measurements of backscattered ultraviolet radiation is examined. Using radiative transfer calculations, we show that the radiative effects of UV-absorbing aerosols produce spurious ozone column reductions. The magnitude of the total ozone underestimation depends on the aerosol type, optical depth, and aerosol layer height. Desert dust can produce errors as large as 10%. Smaller errors are produced by carbonaceous aerosols that result from biomass burning. Ozone retrieval errors associated with nonabsorbing aerosols are typically ±1% of the total ozone amount depending on aerosol optical depth and viewing geometry. Though the error is produced by complex interactions between ozone absorption (both stratospheric and tropospheric), aerosol scattering, and aerosol absorption, a surprisingly simple correction procedure reduces the error to ~1% for a variety of aerosols and for a wide range of aerosol loading. Comparison of the corrected Total Ozone Mapping Spectrometer (TOMS) data with operational data indicates that though the zonal mean total ozone derived from TOMS is not significantly affected by these errors, localized effects in the tropics can be large enough to affect seriously the studies of tropospheric ozone that are currently undergoing using the TOMS data.

1. Introduction

The inversion of satellite measured backscattered ultraviolet (BUV) radiances has proven to be an extremely reliable method of globally mapping the spatial and temporal distribution of the atmospheric ozone content. Since the first space-borne BUV sensor was launched in 1970, several ozone sensing experiments (Total Ozone Mapping Spectrometer (TOMS), solar backscattered ultraviolet (SBUV) and Global Ozone Monitoring Experiment (GOME)) have used observations of the BUV radiation to monitor continuously the stratospheric ozone layer. Most future satellite missions to study the ozone layer are expected to include BUV-based ozone sensors. It was recognized very early [*Dave*, 1978] that the scattering and absorption effects of aerosols (both tropospheric and stratospheric) modify the ultraviolet radiation field and affect the retrieval of total ozone content and its vertical distribution. Though the impact of background stratospheric aerosols on the ozone retrieval is small, large volcanic eruptions such as El Chichon (1982) and Mount Pinatubo (1991) produce easily recognizable artifacts in the total ozone field [*Bhartia et al.*, 1993; *Torres et al.*, 1995] and in the retrieved vertical distribution [*Mergenthaler*, 1985; *Torres and Bhartia*, 1995].

This paper discusses the effect that tropospheric aerosols have on the TOMS ozone retrieval process. Though earlier studies [e.g., *Dave*, 1978] looked at this problem, they used a limited number of synthetic aerosol models that were not tied to particular types of aerosols found in the Earth's atmosphere. A fresh look at the problem has become important for two reasons: (1) a new method of mapping aerosols using TOMS measurements has become available [*Torres et al.*, 1998; *Herman et al.*, 1997], and (2) residual techniques applied to the TOMS data are now also utilized to infer tropospheric ozone content [*Fishman et al.*, 1990; *Hudson and Thompson*, 1998; *Ziemke et al.*, 1998]. Since tropospheric ozone is ~10% of the total ozone, a small error in total ozone can propagate to the derived tropospheric ozone, yielding a much larger percent error in the derived tropospheric ozone content. Moreover, most of the studies of tropospheric ozone focus on precisely the areas where the atmosphere has a large aerosol loading due to biomass burning or other pollution episodes.

We begin with an analysis of the effect of tropospheric aerosol types on the BUV radiances in section 2. The resulting errors in retrieved ozone are examined in section 3 by using synthetic aerosol-contaminated radiances in the TOMS algorithm. Finally, a method to correct for the tropospheric aerosol effect is discussed.

2. Tropospheric Aerosol Effect on Backscattered Radiances

2.1. Aerosol Models

A set of aerosol models representative of the most abundant tropospheric aerosol types were selected for this analysis. Table 1 shows the refractive index and the parameters (mode radius and width) of the aerosol models lognormal particle size distribution [*Torres et al.*, 1998]. Nonabsorbing tropospheric aerosols of anthropogenic origin are represented by a sulfate aerosol model [*Shaw*, 1979] denoted by S in Table 1. Model C1 represents weakly UV-absorbing carbonaceous particulate representative of aerosol material from the smoldering phase of combustion. It is the most abundant aerosol type in regions

[1]Also at Joint Center for Earth Science Technology, University of Maryland, Baltimore.

Paper number 1999JD900410.
0148-0227/99/1999JD900410$09.00

Table 1. Aerosol Models Used in the Simulation Study

Aerosol Model		Parameters		Refractive Index (380 nm)
Symbol	Description	r_0	σ	
S	nonabsorbing aerosols	0.07	2.03	1.43–0.000i
C1	weakly UV-absorbing carbonaceous aerosols	0.14	1.45	1.55–0.015i
C2	moderately UV-absorbing carbonaceous aerosols	0.14	1.45	1.55–0.035i
D	UV-absorbing mineral dust	0.25	2.20	1.57–0.015i

The refractive index for models S, C1, and C2 is assumed to be wavelength-independent. The spectral dependence of the D model refractive index is taken from *Patterson et al.* [1977].

where intensive biomass burning takes place on a seasonal basis. Model C2 is representative of the more absorbing carbonaceous aerosol particles associated with the flaming phase of the fire generally found near the source region. Since data on the refractive index of carbonaceous aerosols in the UV are not available, its spectral dependence is not taken into account, and the assumed values in Table 1 are based on measurements in the visible [*Patterson and McMahon*, 1984]. Model D represents strongly absorbing desert dust aerosols. The spectrally dependent refractive index of the D model is taken from measurements of Saharan desert dust absorption by *Patterson et al.* [1977].

The aerosol vertical distribution of the absorbing aerosols is assumed to be a Gaussian distribution characterized by the height of maximum aerosol concentration (peak of the distribution) and its half width. The nonabsorbing aerosol vertical distribution is assumed to be maximum at the surface and to decrease exponentially with height. Calculations were done for several values of aerosol optical depth and aerosol layer altitude. Low-latitude ozone profiles [*McPeters et al.*, 1996] with integrated ozone contents of 275 and 325 Dobson units (DU) were assumed. The effect of each aerosol model was analyzed separately; that is, no aerosol mixtures were considered.

Synthetic aerosol-contaminated radiances were used to simulate the intensities measured from space when the atmosphere contains suspended particulate represented by the aerosol models in Table 1 for an optical depth of 1.0 (at 380 nm). For the sulfate aerosol model (S) an optical depth of 1.0 should be regarded as representative of the most severe cases of tropospheric sulfate contamination. For carbonaceous and mineral aerosol models this value of optical depth can be considered typical. Optical depths of 1.0 and larger are commonly observed during the large-scale biomass burning events known to take place seasonally in South America [*Gleason et al.*, 1998] and Equatorial Africa. Sunphotometer measurements of desert dust aerosols periodically report values in excess of 1.0 during dust outbreaks [*Pinker et al.*, 1994; *D'Almeida*, 1987; *Faizoun et al.*, 1994].

2.2. Spectral Dependence of the Aerosol Effect

In addition to aerosol physical properties (particle size distribution and complex refractive index), the change in upwelling ultraviolet radiance at the top of an aerosol-laden atmosphere also depends on the aerosol optical depth, its location in the atmosphere, and the reflectivity of the underlying surface. The change in radiance, with respect to a molecular atmosphere with a vertically distributed ozone amount, is shown in Figure 1 for the aerosol models used in this work (solid lines). The transition from a radiance increase at all wavelengths for the nonabsorbing sulfate aerosol model to a radiance decrease for the highly absorbing mineral dust model is produced by the competing effects of scattering and absorption by the particles. A detailed discussion of the dependence of the aerosol effect on other factors such as altitude of the aerosol layer and reflectivity of the underlying surface is presented by *Torres et al.* [1998].

The aerosol effect in the 340–380 nm range is approximately linear with wavelength for all aerosol models. The slight nonlinearity of the D model is related to the spectrally dependent imaginary component of the refractive index used in the calculations. A clear departure from linearity is observed at wavelengths shorter than ~340 nm. This deviation from linearity is not directly associated with the aerosol spectral optical properties. Rather, it is the result of the complex interaction of the scattering and absorption (by ozone and aerosols) processes of both Rayleigh and Mie scattered photons. This is clearly illustrated by the dashed lines in Figure 1, which show that when the atmosphere does not contain ozone, the linearity of the aerosol effect extends to the 310–340 spectral range.

3. Aerosol Impact on TOMS Ozone Retrieval

In this section we present quantitative estimates of the errors introduced by aerosols in the ozone amounts retrieved

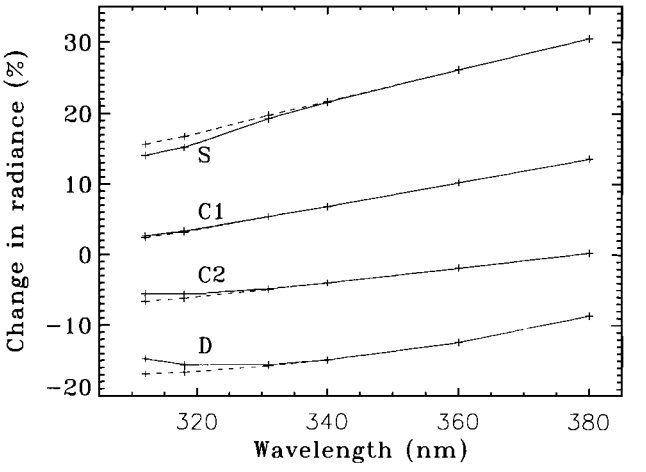

Figure 1. Spectral dependence of the change in backscattered radiance with respect to a molecular atmosphere with ozone absorption for the four aerosol models in Table 1 (solid lines). The obtained spectral dependence when the atmosphere does not contain ozone is shown by the dashed lines. The symbols indicate the wavelengths of the calculations. The aerosol optical depth (at 380 nm) is set to unity, and the absorbing aerosol layer is placed at 3.0 km. Other assumed conditions are ozone content, 275 Dobson units (DU); reflectivity of the surface, 0.05; solar zenith angle, 20°; and nadir viewing.

from satellite measurements of BUV radiation using the TOMS algorithm. A very short and simple description of the TOMS algorithm follows. For a more detailed discussion of the TOMS ozone retrieval process the reader is advised to see *McPeters et al.* [1996].

3.1. TOMS Algorithm

The current operational (version 7) TOMS total ozone algorithm is essentially a two-step process. In the first step an initial estimate of total ozone is obtained by assuming a "Rayleigh model" of the atmosphere. In this model one approximates the true atmosphere by a molecular atmosphere containing a vertically distributed ozone amount bounded at the bottom by a Lambertian reflecting surface. For clear-sky conditions, or for fully cloudy scenes containing optically thick clouds, the reflectivity of the surface is adjusted to match the measured radiances at one wavelength (generally 360 or 380 nm), called the reflectivity wavelength (λ_R). For scenes containing broken clouds, radiances are obtained by linearly mixing the cloudy and clear scenes (using nominal values of surface and cloud reflectivities) to match the radiances at λ_R. (For further details the readers are referred to the relevant TOMS user guides [e.g., *McPeters et al.*, 1996].) The algorithm predicts the radiances at other TOMS wavelengths by detailed radiative transfer computations that account for ozone absorption, multiple scattering and polarization effects, Earth's sphericity effects, surface reflection, and the effects of instrument bandpass and atmospheric temperature. A simple correction is applied for rotational Raman scattering (ring effect) using the model developed by *Joiner et al.* [1995]. By interpolation of precomputed tables that vary with latitude and total ozone amount the algorithm finds a value of total ozone that explains the ratio of measured radiances at a pair of wavelengths (317.5 and 331.2 nm).

Careful analysis of TOMS data at weakly ozone-absorbing wavelengths (>330 nm) indicated that though the Rayleigh model (RM) worked surprisingly well in most cases, there were some notable exceptions. These included highly non-Lambertian surfaces (e.g., sea glint), UV-absorbing aerosols (volcanic ash, smoke, and mineral dust), and small-size non-absorbing aerosols. A detailed study of these deviations from the RM has led to the discovery of a fundamental new technique for detecting tropospheric aerosol from space [*Herman et al.*, 1997; *Torres et al.*, 1998]. To account for these effects (as well as for the selection of a better ozone profile, which will not be discussed here), the version 7 TOMS algorithm includes a second step. A quantity called residue is calculated as the difference in the logarithm of the measured radiances (historically referred to as N value) and those calculated from the RM. The N value definition of residue is nearly equal to the percentage difference between the measured and the predicted radiances divided by -2.3. Note that by definition of the RM the λ_R residue is zero. In the retrieval algorithm the residue is assumed to be linear with wavelength. Ozone is then recalculated by applying this correction using a first-order Taylor series expansion around the previously calculated ozone value [see *McPeters et al.*, 1996]. The key point to note is that for this correction to be accurate the residues must be linear with wavelength. We examine this assumption next. There are additional sources of uncertainty in the ozone retrieval (for instance, ozone profile shape, loss of sensitivity to tropospheric ozone, and sun glint), which are additive and contribute to the spectral residues. At low and moderate solar zenith angles, however, the largest source of error is the presence of aerosols. The analysis of sensitivities to error sources other than aerosols is out of the scope of this paper.

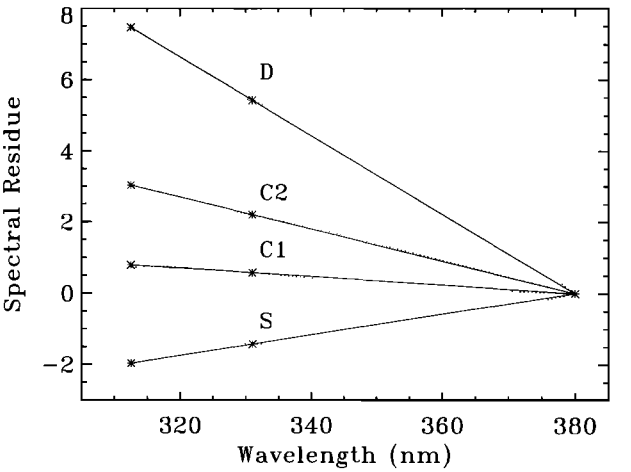

Figure 2. Residues (see text) as a function of wavelength for the aerosol models used in the analysis (dotted lines). The solid straight lines represent the algorithm assumed spectral dependence of the residual quantities. All modeling conditions are the same as in Figure 1.

3.2. Simulation Experiment

A simulation study was conducted in order to quantify the error in the retrieved ozone column amount when the atmosphere is loaded with aerosol particles. Radiative transfer calculations at the TOMS wavelengths were performed to generate the aerosol-contaminated radiances emanating at the top of an atmosphere of known total ozone content. Calculations were carried out for the aerosol models discussed in section 2. To evaluate the aerosol effect under different conditions, radiative transfer calculations were done for several values of the 380 nm aerosol optical depth (0.5, 1, 2, and 4) and different locations of the aerosol layer (0.5, 1.5, 3, and 6 km) above the ground. The aerosol and ozone vertical distribution were discussed in section 2.

The aerosol-contaminated radiances were input to the TOMS algorithm. The difference between the retrieved ozone amount and the actual ozone content is the retrieval error associated with the aerosol interference. The error is expressed in percent of the total ozone amount. Calculations using different total ozone amounts indicate that although the absolute error increases with increasing total ozone amount, the relative or percent error does not depend on the total ozone content provided that the tropospheric component of the total ozone column does not change with changing total ozone content. The implication of tropospheric ozone variability in the resulting retrieval error will be discussed in a subsequent section.

Since in the simulation analysis the true atmospheric ozone content is known the spectral dependence departure (from a molecular atmosphere) shown in Figure 2 (dashed lines) in terms of residues is computed. The results reflect the interaction of the several radiative transfer processes taking place in the atmosphere: molecular and particle scattering as well as absorption by ozone molecules and aerosol particles of both Rayleigh- and Mie-scattered radiation. Also shown are the residues predicted by the TOMS algorithm at 312.5, 331.2, and

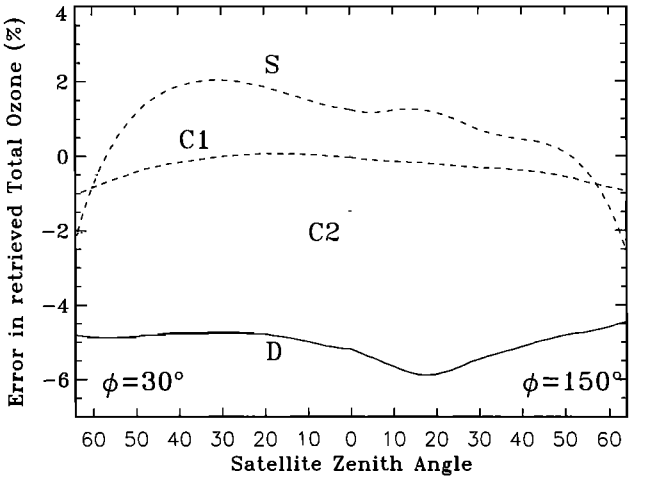

Figure 3. Percent error in retrieved total ozone as a function of satellite zenith angle for the set of assumed aerosol models at relative azimuth angles typical of a Sun synchronous orbit at low latitudes. Other modeling conditions are as in Figure 1.

380 nm. Residues associated with nonabsorbing aerosols (model S) are negative, whereas positive residues are generally associated with absorbing particulate [*Torres et al.*, 1998]. The straight solid lines are obtained by assuming a linear dependence of the residues in the 331–380 range and extrapolation to 312.5 nm. Although the linear function is a good representation of the wavelength dependence of the residues produced by weakly absorbing aerosols (model C1), there is a significant departure from linearity for highly absorbing and nonabsorbing aerosols. Because of this, when the atmosphere is loaded with highly absorbing aerosols, the retrieved ozone amount is in error.

3.3. Angular Dependence of the Aerosol Effect

The simulated ozone retrieval error for the aerosol models used in this analysis are shown in Figure 3 for typical TOMS viewing conditions. In general, the effect of the nonabsorbing aerosol particles (model S) is to induce a scan angle dependent ozone overestimation of up to ~2%. As the satellite zenith angle increases beyond 50°, the error decreases, becoming negative (−2%) at the extreme TOMS satellite zenith angles. The angular dependence is associated with the aerosol-scattering phase function. The above error estimates correspond to an aerosol layer of unusually high optical depth of 1. For a more representative near-UV optical depth (0.5), typical ozone errors produce by nonabsorbing aerosols are ±1%. The dependence on the height of the nonabsorbing layer is negligible. The angular dependence of the carbonaceous aerosol models (C1 and C2) is not as pronounced, whereas the mineral aerosol model (D) shows a well-defined scan angle variability.

3.4. Effect of Aerosol Absorption

The error in the retrieved ozone amount in the presence of absorbing particles increases with increasing aerosol optical depth and height of the absorbing aerosol layer. Contours illustrating the resulting ozone artifact as a function of aerosol optical depth and layer height are shown in Figure 4. The sign of the ozone error resulting from the presence of weakly absorbing particles (model C1) depends on the combined effect of the aerosol layer optical depth and its altitude above the surface. As shown in Figure 4a, small (<1%) positive errors are produced by aerosol layers located as high as 2 km above the surface and having optical depths as large as 2.0. Aerosol layers higher than ~3 km or with optical depths larger than ~3 are required to produce negative errors. Thus, for realistic conditions with aerosol optical depths of large as 3 and aerosol layer locations of 3 km the ozone error due to C1 aerosols is ~−1%.

The more absorbing carbonaceous aerosol model (C2) produces predominantly negative errors except when the aerosol layer lies a few hundred meters above the surface, as shown in Figure 4b. Ozone underestimations between 3 and 4% are possible for aerosol layers at 3 km and optical depths of 3 or larger. The effect of strongly absorbing mineral aerosols (model D) on the ozone retrieval is shown by the contour plot in Figure 4c. This aerosol type yields negative ozone amount errors regardless of aerosol optical depth and location in the atmosphere. For typical optical depth values between 1 and 2 and aerosol layer heights between 3 and 5 km, ozone amount errors as large as 10% are possible.

3.5. Error Sources

In this section we examine the causes of the aerosol errors we have just discussed. From Figure 1 we already know that the linear model assumed by the TOMS version 7 algorithm is correct in the absence of atmospheric ozone, but it becomes inaccurate when ozone is added. To examine whether the effect is primarily due to a change in the effective tropospheric air mass factor (photon path length) due to interaction between tropospheric ozone and aerosols, we ran our mineral dust model with and without tropospheric ozone. These results, shown in Figure 5, indicate that 50–75% of the ozone error remains even in the absence of tropospheric ozone even for aerosols close to the surface. Since aerosols so low in the atmosphere cannot directly alter the path of photons in the stratosphere, the error results from the fact that ozone reduces the number of photons reaching the troposphere and hence interacting with aerosols. The remaining error (shown by the dotted line), attributable to tropospheric ozone, is probably due to a change in the path of the photons in the troposphere due to aerosols. Part of this simply is a shielding effect; that is, a highly absorbing layer would partially shield the ozone below it. However, the fact that the dotted line does not go to zero for very low altitude aerosols indicates that the absorption of photons by ozone above the aerosol layer is also reduced. This is probably because there is less multiple scattering in the presence of absorbing aerosols than in the Rayleigh atmosphere.

The foregoing discussion highlights the fact that the effect of aerosols on BUV radiation is strongly affected by atmospheric ozone and hence cannot be corrected by any form of monotonic correction scheme, linear or otherwise. This has implications for other methods of retrieving ozone from BUV radiances, for example, the differential optical absorption spectroscopy (DOAS) method used in processing the GOME BUV data [*European Space Agency*, 1995].

4. Correction Procedure

Because the aerosol effect on the BUV radiation depends on several different parameters (complex refractive index, particle size distribution, aerosol optical depth, and aerosol layer height), it is extremely difficult to correct accurately the measured BUV radiances for the radiative transfer effects of aero-

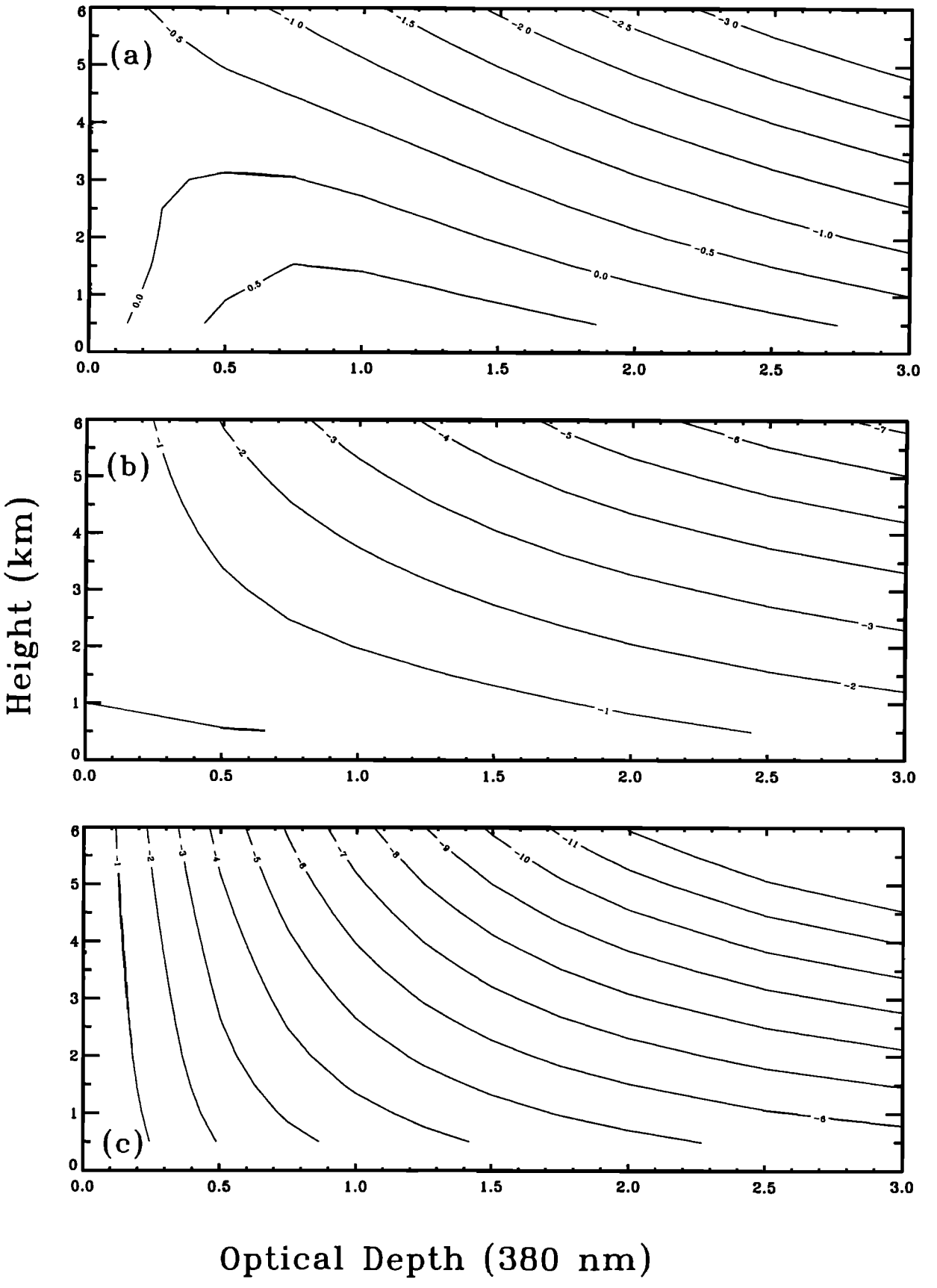

Figure 4. Contours describing the ozone error (in percent) introduced by absorbing aerosols as a function of the aerosol optical depth and aerosol layer height above the ground: (a) weakly absorbing carbonaceous aerosols (model C1), (b) moderately absorbing carbonaceous aerosol (model C2), and (c) mineral dust (model D). Other modeling conditions are as in Figure 1.

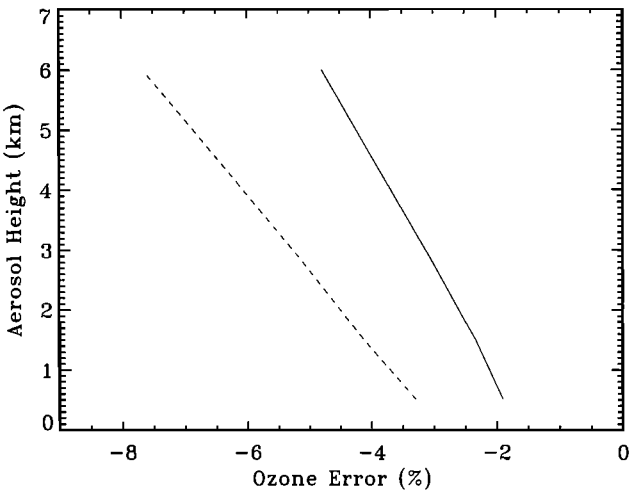

Figure 5. Percent ozone retrieval error as a function of aerosol layer height for the mineral aerosol model (D) of optical depth 1.0 (dashed line). The dotted line represents the component of the total error associated with the "ozone-masking" effect of the aerosol layer (see text). The solid line represents the part of the total error resulting from the error in predicting the spectral dependence of the aerosol effect on the backscattered radiances.

sols. The difficulty lies in the fact that required information on the aerosol properties and vertical distribution is generally unavailable.

To search for a simple correction scheme, we examined the relationship between the ozone error and the aerosol index (AI), which is simply the 340 nm (331 nm for EP/TOMS) residue in N value units. (If the residues are defined using the natural logarithm, N value, obtained by multiplying it with $-100 \log_{10}(e)$, converts it into a more convenient unit.) On the basis of *Herman et al.* [1997] and *Torres et al.* [1998] we know that AI provides a convenient way of tracking aerosols all over the globe. UV-absorbing aerosols are associated with positive AI values, whereas nonabsorbing small-size ($<\sim 0.2$ μm) aerosols generally yield negative AI values. Larger nonabsorbing particles produce AI values close to zero. The magnitude of the AI for absorbing aerosols also depend on the altitude of the layer. No such dependence exists for nonabsorbing aerosols. Figure 6 shows the ozone error for the C1, C2, and D models used in this analysis as a function of AI for different heights of the aerosol layer. As illustrated in Figure 6a for aerosol model C1, at a fixed aerosol layer height both the ozone retrieval error and the magnitude of the AI increase with increasing aerosol optical depth. The slope of the ozone error–AI relationship shows only a slight variation for different heights of the aerosol layer. Results of similar analysis for aerosol models C2 and D are illustrated in Figures 6b and 6c, respectively. In spite of the somewhat larger variability of the ozone error–AI relationship with aerosol layer height for model D the observed relationship is very similar for all the aerosol models.

For other viewing geometries the ozone error–AI relationship for the absorbing aerosol models does not deviate significantly from the linear function in Figure 6. For the nonabsorbing aerosol model, however, the ozone error–AI relationship does vary significantly with geometry. As shown in Figure 3, the ozone error can be either negative or positive depending on the geometry of the observation. The variability associated with aerosol type, optical depth, aerosol layer height, and viewing geometry is shown on the scatter plot in Figure 7 for both UV-absorbing and nonabsorbing aerosols. From this analysis it is apparent that the relationship between the retrieval error and AI for the UV-absorbing aerosol models (crosses) is general enough, over a wide range of conditions, to be described mathematically by a simple linear function. The straight solid line shown in Figure 7 was obtained by linearly fitting the data associated with the UV-absorbing aerosol models. The dotted lines indicate the $\pm 1\%$ departure of the ozone error from the linear fit. The few data points slightly outside the $\pm 1\%$ envelope correspond to near-nadir ozone retrievals in the presence of large amounts of dust aerosols (model D) when the relative azimuth angle (i.e., the angle between the planes containing the Sun and the satellite and the instrument field of view) is close to 180°. In practice, this viewing geometry is very infrequent for the near-noon local equator crossing time satellites used by the TOMS sensors.

The same linear function adequately represents the relationship between the ozone overestimation associated with nonabsorbing aerosols (triangles in Figure 7) and negative values of the AI at most viewing configurations. The few data points

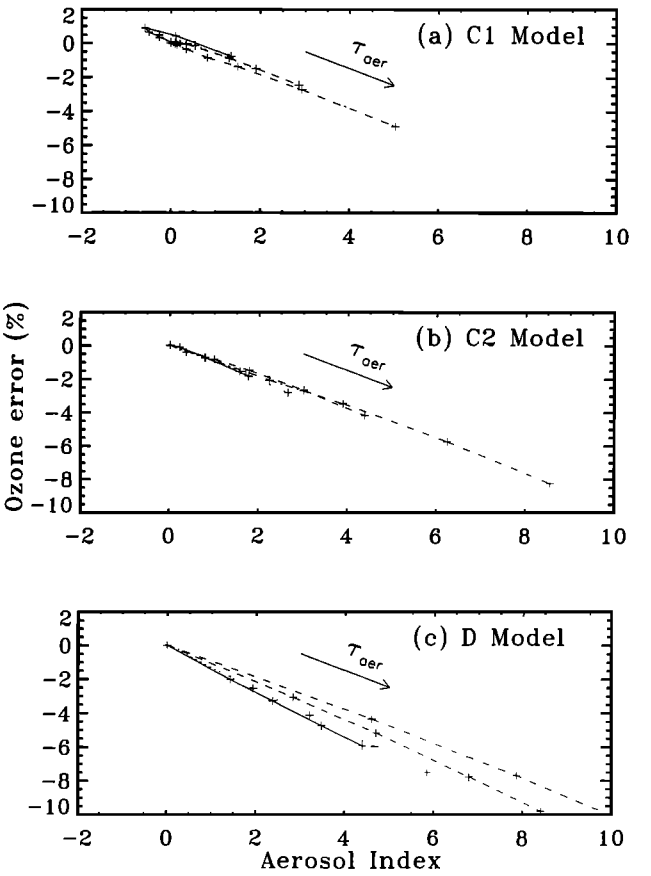

Figure 6. Relationship between the percent ozone error and the Total Ozone Mapping Spectrometer (TOMS) measured aerosol index (AI) for (a) the C1 model, (b) the C2 model, and (c) the D model. The lines represent different heights of the aerosol layer: solid line, 0.5 km; dotted line, 1.5 km; dashed line, 3 km; and dash-dotted line, 6 km. The symbols correspond to calculations for optical depth values of 0, 0.5, 1, 2, and 4, increasing in the direction of the arrow.

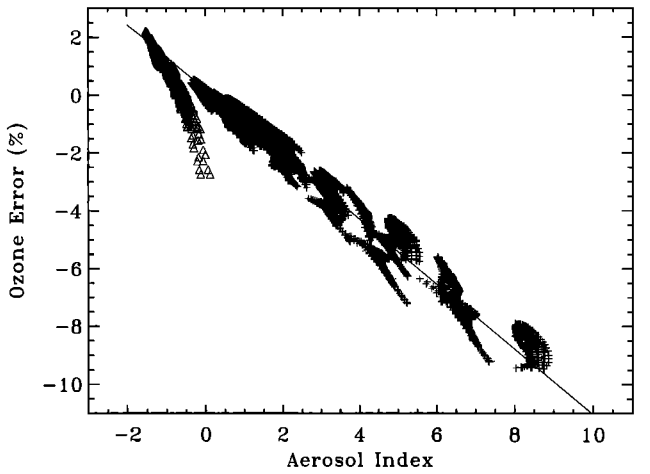

Figure 7. Scatter plot illustrating the variability of the ozone error–AI relationship for simultaneously changing aerosol type, aerosol layer height (0.5, 1.5, 3, and 6 km), aerosol optical depth (0.5, 1.0, 2.0, and 4.0); relative azimuth angle (0°–180°, 30° steps), and satellite zenith angle (0°–64°, 2° steps). The pluses represent UV-absorbing aerosols (models C1, C2, and D), and the triangles correspond to nonabsorbing particles (model S). Also shown is the linear fit to the synthetic data points. The two dotted lines represent the ±1% deviation from the linear fit.

outside the 1% range are retrievals at extreme off-nadir geometries (i.e., satellite zenith angles >58°) in the presence of large amounts of nonabsorbing particles.

The well-defined relationship between the AI and the aerosol artifact in the retrieved ozone amount can be used to apply a first-order correction to the ozone product. This correction method does not require any information on the aerosol microphysical properties or location in the atmosphere. An additional advantage is that such a correction can easily be applied to the retrieved ozone amounts without requiring knowledge of the specific viewing geometry.

On the basis of the previous discussion the ozone artifact (in Dobson units) associated with the presence of tropospheric aerosols is

$$\varepsilon = 0.01k\mathrm{AI}\Omega_{\mathrm{ret}}, \quad (1)$$

where Ω_{ret} is the retrieved ozone amount, AI is the aerosol index, and k is the slope of the linear fit in Figure 7. The value of k is 1.12 for the 340–380 AI and 1.20 for the 331–360 AI (used for Earth Probe and ADEOS TOMS sensors). As shown by the dotted lines in Figure 7, the application of (1) reduces the aerosol-related artifact in the ozone retrieval to ±1% under most conditions.

5. Aerosol Effect on Nimbus 7-TOMS Data

Validation of the above described relationship in the TOMS data is not direct since the ozone variability associated with the aerosol interference must be separated from the natural spatial and temporal variability of the tropospheric ozone field. The natural variability may include tropospheric ozone increases as a biomass burning by-product and possible reductions as result of ozone processing on the surface of mineral dust aerosols [*Dentener et al.*, 1996]. Additional ozone reductions or enhancements may occur in the vicinity of the aerosol layer as the interaction of the aerosol scattering and absorption processes affect the ozone photolysis rates [*Jacobson*, 1998]. Unfortunately, the necessary information, both theoretical and observational, required to account for the actual tropospheric ozone variability is not available. Since those effects are quite probably similar in magnitude to the aerosol-introduced artifact (i.e., a few Dobson units), the results of a validation effort would be inconclusive.

A qualitative verification of the relationship between the absorbing aerosol-induced ozone underestimation and the AI is observed over the Saharan Desert. The effect is more easily observed during the summer when the aerosol layer is generally higher (~4 km or more above the surface), yielding larger AI values for the same amount of aerosol. These regions of high AI are frequently associated with total ozone amounts lower than in neighboring areas where the aerosol presence, as detected by the AI, is not as strong.

Over the biomass burning areas, on the other hand, the verification of the theoretically derived ozone error–AI relationship is more complicated. Although some areas of reduced ozone and large AI can be found, there are areas where the ozone content is enhanced in relation to the surrounding areas in spite of large AI values. A likely explanation of this reverse correlation is that the natural ozone increase generally associated with biomass burning events could be offsetting the aerosol absorption artifact.

Plate 1 shows the global geographical distribution of the error in the TOMS-derived ozone field on August 23, 1985, as obtained using (1). As expected, the retrieval errors are localized over the arid regions of the world and over areas known to be affected by large-scale biomass burning such as South America and Central Africa. On this particular day, derived errors as large as 5% (~14 DU) are observed over the western Saharan Desert, the coast of Angola, and Brazil. The effect of the aerosol artifact on the zonally averaged total ozone data is negligible (<1%).

6. Summary and Conclusions

The radiative transfer processes of aerosol scattering and absorption affect the retrieval of ozone column amount by the TOMS sensor. The algorithm-predicted linear spectral dependence of the effect of nonabsorbing and weakly absorbing particles on the backscattered radiances is very close to the observed wavelength dependence. For this reason the ozone retrieval error in the presence of nonabsorbing sulfate and weakly absorbing carbonaceous aerosols is small. The deviation of the observed spectral dependence from the algorithmic assumption is larger when the atmosphere is loaded with moderately absorbing carbonaceous particulate and highly absorbing mineral dust. This causes significantly larger errors to occur.

The absorbing aerosol–induced error consists of a pseudoreduction of the atmospheric ozone column over those areas where large amounts of absorbing aerosols are present at 2 km or higher in the atmosphere. The retrieval error increases with increasing aerosol optical depth and aerosol layer height. The ozone underestimation due to the effect of biomass burning aerosols are generally small (2% or less) since smoke layers generally reside in the lowest 2 km of the atmosphere. Only when the smoke layer rises significantly or is present in large amounts are errors larger than 2% expected. On the other

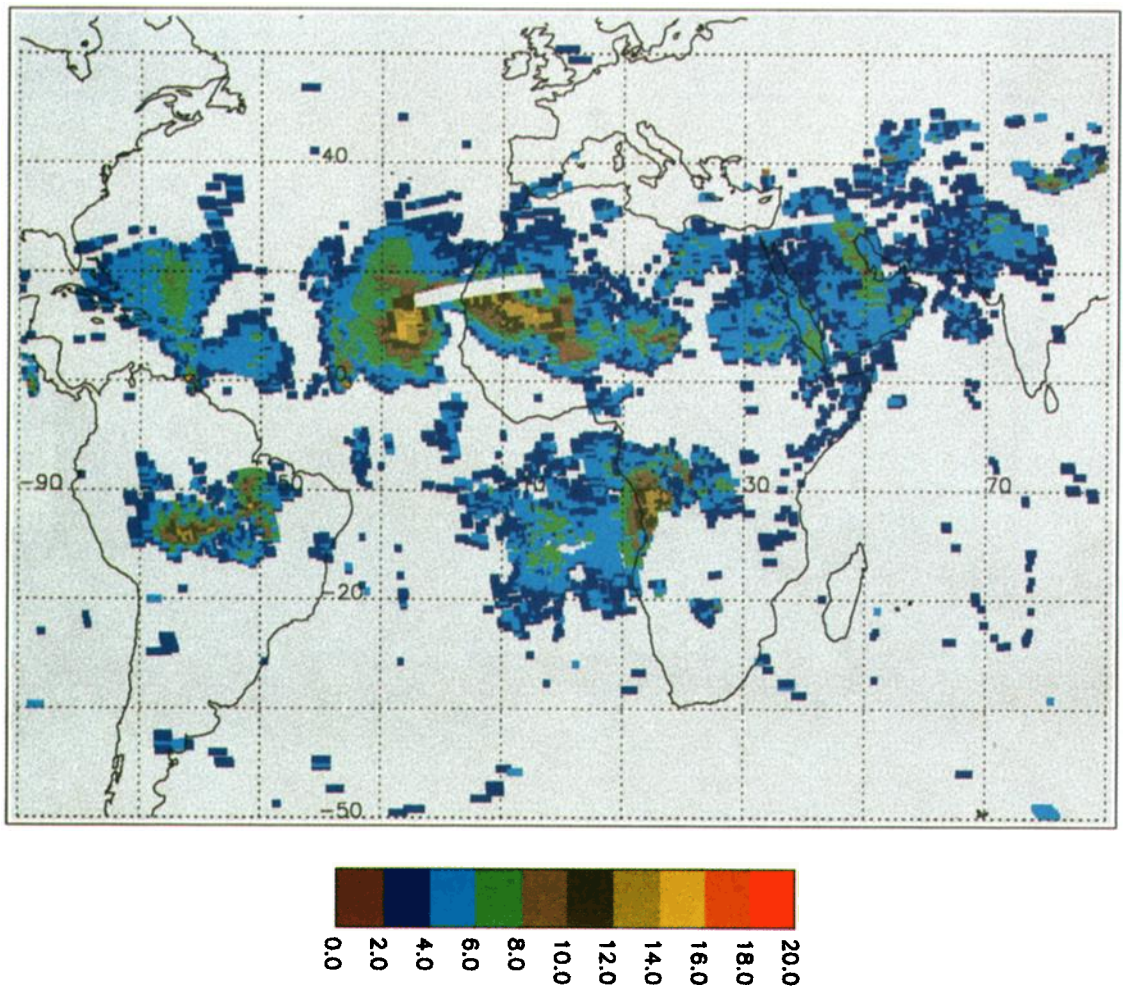

Plate 1. Global geographical distribution of the underestimation in Nimbus 7-TOMS retrieved total ozone amount (in Dobson units) on August 23, 1985, as derived by making use of the TOMS-derived aerosol index.

hand, errors as large as 8% are produced by layers of desert dust at 4 km or higher.

The close linear relationship between the ozone error associated with absorbing aerosols and the TOMS aerosol index is the most important finding of this work. It has been shown that regardless of the aerosol type, optical depth, aerosol layer height, and viewing geometry, there exists a well-defined linear relationship between the error (as a percent of the total column amount) and the value of the aerosol index. This relationship is general enough to allow the application of a first-order correction to the ozone data. Because the variability associated with the viewing geometry is small, the correction can be applied directly to the level 3 gridded data. The corrected ozone data are within 1% of the true value.

Correcting the ozone retrieval for the aerosol effect reduces the uncertainty of the tropospheric ozone content derived as a difference between the TOMS total ozone and other independent estimates of the stratospheric ozone content. The use of uncorrected TOMS total ozone amounts, in the application of the residual techniques, results in spurious tropospheric ozone deficits.

Acknowledgments. We thank L. Moy of Raytheon STX Corporation for her assistance with radiative transfer calculations.

References

Bhartia, P. K., J. R. Herman, R. D. McPeters, and O. Torres, Effect of Mount Pinatubo aerosols on total ozone measurements from backscatter ultraviolet (BUV) experiments, *J. Geophys. Res.*, *98*, 18,547–18,554, 1993.

d'Almeida, G. A., On the variability of desert aerosol radiative characteristics, *J. Geophys. Res.*, *92*, 3017–3026, 1987.

Dave, J. V., Effects of aerosols on the estimation of total ozone in an atmospheric column from the measurements of its ultraviolet radiance, *J. Atmos. Sci.*, *35*, 899–911, 1978.

Dentener, F. J., G. R. Carmichael, Y. Zhang, J. Lelieveld, and P. J. Crutzen, Role of mineral aerosol as a reactive surface in the global troposphere, *J. Geophys. Res.*, *101*, 22,869–22,889, 1996.

European Space Agency, *Global Ozone Monitoring Experiment Users Manual*, Noordwijk, Neth., 1995.

Faizoun, C. A., A. Podaire, and G. Dedieu, Monitoring of sahelian aerosol and atmospheric water vapor content characteristics from Sun photometer measurements, *J. Appl. Meteorol.*, *33*, 1291–1303, 1994.

Fishman, J., C. E. Watson, J. C. Larsen, and J. A. Logan, Distribution of tropospheric ozone determined from satellite data, *J. Geophys. Res.*, *95*, 3599–3617, 1990.

Gleason, J. F., N. C. Hsu, and O. Torres, Biomass burning smoke measured using backscattered ultraviolet radiation: SCAR-B and Brazilian smoke interannual variability, *J. Geophys. Res.*, *103*, 31,969–31,978, 1998.

Herman, J. R., P. K. Bhartia, O. Torres, N. C. Hsu, C. J. Seftor, and E.

Celarier, Global distribution of UV-absorbing aerosols, *J. Geophys. Res.*, *102*, 16,911–16,922, 1997.

Hudson, R. D., and A. M. Thompson, Tropical tropospheric ozone from total ozone mapping spectrometer by a modified residual method, *J. Geophys. Res.*, *103*, 22,129–22,145, 1998.

Jacobson, M. Z., Studying the effects of aerosols on vertical photolysis rate coefficient and temperature profiles over an urban airshed, *J. Geophys. Res.*, *103*, 10,593–10,604, 1998.

Joiner, J. P., P. K. Bhartia, R. P. Cebula, E. Hilsenrath, and R. D. McPeters, Rotational Raman scattering (ring effect) in satellite backscatter ultraviolet measurements, *Appl. Opt.*, *34*, 4513–4525, 1998.

McPeters, R. D., et al., Nimbus 7 Total Ozone Mapping Spectrometer (TOMS) data products user's guide, *NASA Ref. Publ.*, *1384*, 67, 1996.

Mergenthaler, J. L., An estimate of the effect of El Chichon aerosol on SBUV profiling for summer 1982, *J. Geophys. Res.*, *90*, 2355–2359, 1985.

Patterson, E. M., and C. K. McMahon, Absorption characteristics of forest fire particulate matter, *Atmos. Environ.*, *18*, 2541–2551, 1984.

Patterson, E. M., D. A. Gillette, and B. Stockton, Complex index of refraction between 300 and 700 nm for sharan aerosols, *J. Geophys. Res.*, *82*, 3153–3160, 1977.

Pinker, R. T., G. Idemudia, and T. O. Aro, Characteristic aerosol optical depths during the Harmattan season on sub-Sahara Africa, *Geophys. Res. Lett.*, *21*, 685–688, 1994.

Shaw, G. E., Considerations on the origin and properties of the Antarctic aerosol, *Rev. Geophys.*, *17*, 1983–1998, 1979.

Torres, O., and P. K. Bhartia, Effect of stratospheric aerosol on ozone profile from BUV measurements, *Geophys. Res. Lett.*, *22*, 235–238, 1995.

Torres, O., J. R. Herman, P. K. Bhartia, and Z. Ahmad, Properties of Mount Pinatubo aerosols as derived from NIMBUS 7 total ozone mapping spectrometer measurements, *J. Geophys. Res.*, *100*, 14,043–14,055, 1995.

Torres, O., P. K. Bhartia, J. R. Herman, Z. Ahmad, and J. Gleason, Derivation of aerosol properties from satellite measurements of backscattered ultraviolet radiation: Theoretical basis, *J. Geophys. Res.*, *103*, 17,099–17,110, 1998.

Ziemke, J. R., S. Chandra, and P. K. Bhartia, Two new methods for deriving tropospheric column ozone from TOMS measurements: The assimilated UARS MLS/HALOE and convective-cloud differential techniques, *J. Geophys. Res.*, *103*, 22,115–22,128, 1998.

P. K. Bhartia and O. Torres, Laboratory for Atmospheres, NASA Goddard Space Flight Center, Code 916, Greenbelt, MD 20771. (torres@tparty.gsfc.nasa.gov)

(Received November 17, 1998; revised June 7, 1999; accepted June 8, 1999.)